Carbohydrate Polymers 296 (2022) 119922

Contents lists available at ScienceDirect

Carbohydrate Polymers

journal homepage: www.elsevier.com/locate/carbpol

Cellulose lattice strains and stress transfer in native and delignified wood

Paul-Antoine Spies [a,b], Tobias Keplinger [a], Nils Horbelt [c], Friedrich Reppe [c], Ernesto Scoppola [c], Michaela Eder [c], Peter Fratzl [c], Ingo Burgert [a,b,*], Markus Rüggeberg [d]

[a] Wood Materials Science, Institute for Building Materials, ETH Zürich, 8093 Zürich, Switzerland
[b] WoodTec group, Cellulose and Wood Materials, Empa – Swiss Federal Laboratories for Materials Science and Technology, 8600 Dübendorf, Switzerland
[c] Department of Biomaterials, Max-Planck-Institute of Colloids and Interfaces, Wissenschaftspark Golm, Am Muhlenberg 1, 14476 Potsdam, Germany
[d] Institute of Forest Utilization and Forest Technology, TU Dresden, 01737 Tharandt, Germany

ARTICLE INFO

Keywords:
Delignified wood
In-situ tensile tests
Stress-transfer
Stress-strain behavior
Cellulose lattice strain

ABSTRACT

Small specimens of spruce wood with different degrees of delignification were studied using in-situ tensile tests and simultaneous synchrotron X-ray diffraction to reveal the effect of delignification and densification on their tensile properties at relative humidities of 70–80 %. In addition to mechanical properties, these analyses yield the ratio of strains in the cellulose crystals and in the bulk, which reflects the stress-transfer to crystalline cellulose. While the specific modulus of elasticity slightly increases from native wood by partial or complete delignification, the lattice strain ratio does not show a significant change. This could indicate a compensatory effect from the decomposition of the amorphous matrix by delignification and from a tighter packing of cellulose crystals that would increase the stress transfer. The reduced strain to failure and maximum lattice strain of delignified specimens suggests that the removal of lignin affects the stress-strain behavior with fracture at lower strain levels.

1. Introduction

Optimized by nature for millions of years, wood is a natural composite material demonstrating outstanding properties considering its low density. Numerous investigators have examined its intricate hierarchical structure from the integral level of the living tree to the polymers composing the wood cell wall, namely cellulose, hemicelluloses and lignin (Conrad et al., 2003; Klauditz, 1952; Stanzl-Tschegg, 2011). Wound helicoidally around the lumen of the wood cell, stiff and strong cellulose microfibrils form aggregates embedded in an amorphous matrix of lignin and hemicellulose in the cell wall (Salmén, 2018). Semi-crystalline cellulose microfibrils are known as the main structural contributor in the cell wall and their microfibril angle (MFA) relative to the longitudinal cell axis greatly influences mechanical properties of wood (Diddens et al., 2008; Keckes et al., 2003; Özparpucu et al., 2019; Salmèn, 2009). Through hydrogen bonding, hemicellulose chains bridge adjacent cellulose microfibrils within aggregates but also act as a connector between aggregates and lignin (Gibson, 2012; Rowell, 2005; Salmén, 2004; Zhang et al., 2021). Determining interactions between the cell wall components, hydrogen bonds play a crucial role in stress transfer between individual polymer chains up to the fiber level (Engelund et al., 2013; Thygesen et al., 2010).

Former works have contributed to further improving the understanding of the mechanical behavior of the cell wall by using advanced characterization techniques (Felhofer et al., 2020; Gierlinger et al., 2006; Salmèn & Bergström, 2009). Moreover, in-situ micromechanical tests combined with methods monitoring structural deformations are a powerful approach to improve the understanding of the mechanical behavior of cell walls (Nakai et al., 2005, 2006). Wide angle X-ray diffraction (WAXD) experiments can determine the local deformation in the crystalline unit cell of crystalline regions in cellulose microfibrils under mechanical load by measuring shifts of the corresponding Bragg reflections (Müller et al., 2011). Keckes et al. in-situ tested wood tissues with high MFAs, thereby collecting valuable information on the mechanical properties of individual cellulose microfibrils as well as on the behavior of the embedding matrix (Keckes et al., 2003). Following similar in-situ approaches, light was shed on local deformation of native cellulose crystals, changes in spatial organization of cell wall polymers under loading as well as on the influence of moisture adsorption on cell wall polymer properties (Diddens et al., 2008; Kamiyama et al., 2005; Kölln et al., 2005; Peura et al., 2007; Salmèn, 2009; Toba et al., 2013; Zabler et al., 2010).

* Corresponding author at: Wood Materials Science, Institute for Building Materials, ETH Zürich, 8093 Zürich, Switzerland.
E-mail address: iburgert@ethz.ch (I. Burgert).

https://doi.org/10.1016/j.carbpol.2022.119922
Received 8 April 2022; Received in revised form 22 July 2022; Accepted 22 July 2022
Available online 28 July 2022

However, further insights are still needed, in particular regarding the stress-transfer mechanisms between cellulose microfibrils and the hemicellulose-lignin matrix. Studies have suggested characterization after partial or complete removal of targeted cell wall components in order to examine their individual-vs-collective mechanical behavior (Jungnikl et al., 2008; Salmén, 2004; Toba et al., 2013). Delignification treatments such as kraft pulping have been used for decades in the paper industry to remove lignin from wood chips in order to obtain cellulosic fibers for paper production. However, such methods are significantly affecting the structural integrity of the bulk material and the cell wall structure. In contrast, structure-retaining delignification techniques preserve the hierarchical structure of wood and the study of the resulting delignified wood can not only help to gain insight into the underlying structure-property relationships of the obtained cellulose materials but could also improve the understanding of stress-transfer mechanisms between cell-wall polymers in general (Frey, Biffi, et al., 2019).

In structure-retaining delignification treatments, the removal of lignin from middle lamellae and cell walls reduces the transverse rigidity of the cell walls and facilitates cell collapse during tangential or radial densification (Shams et al., 2004). Delignified wood can hence undergo densification processes to reach mechanical properties that by far exceed the properties of native untreated wood (Frey et al., 2018; Frey, Biffi, et al., 2019; Keplinger et al., 2020; Song et al., 2018). In addition to the increased density, some studies also suggested that improvement in mechanical performance could be related to the formation of new hydrogen bonds between cellulose microfibrils during densification (Han et al., 2019; Song et al., 2018).

The aim of this work was to investigate the influence of a structure-retaining delignification and eventually subsequent densification on the stress-transfer mechanism at the tissue, cell and cell wall level (between the remaining polymers) at rather high relative humidity (70–80 % RH). Investigations were carried out by in-situ tensile testing and simultaneous synchrotron-powered WAXD on native wood specimens as well as on delignified and also delignified and densified specimens. It is hypothesized that delignification will significantly change the stress transfer at the cell wall level. Lignin as a matrix polymer taking part in the stress transfer at the tissue, cell and cell wall level is degraded and the load-carrying cellulose fibrils may get into more direct contact following delignification. These structural and chemical changes may become visible as an altered ratio of crystalline cellulose strain and bulk strain (for a certain specific elastic modulus) when comparing mechanically loaded native and delignified wood samples. This novel approach of in-situ tensile testing of differently delignified specimens helps to gain further insights into stress-transfer-mechanisms between cellulose fibrils and the surrounding matrix polymers and between cells, and substantially contributes to a deeper understanding of emerging cellulose composite materials.

2. Materials and methods

2.1. Sample preparation

Longitudinal-tangential (LT) sections of Norway spruce (*Picea abies*) with dimensions of 25 × 7 × 0.1 mm^3 (longitudinal × radial × tangential) were prepared with a microtome as illustrated in Fig. 1 from four sample blocks, which were located next to each other within the same growth ring pattern. Preparation and numbering of sections in one growth ring starts with earlywood (the first wood cells formed at the beginning of a growth season in spring) and progresses towards the latewood (wood cells formed towards the end of the growth period). The sections of one wood block were kept in the native, unmodified state (NW), the sections of the other three blocks served as raw material to create i) partially delignified wood (PDW), ii) delignified wood (DW) and iii) delignified and densified wood (DDW).

Following the delignification protocol used by Segmehl et al. and Frey et al., the sections were inserted in a metal-grid sample holder placed in a beaker containing an equal-volume mixture of hydrogen peroxide solution (35 wt%) and glacial acetic acid (Frey et al., 2018; Segmehl et al., 2018). The sections were infiltrated with the mixture over night at room temperature under stirring. The whole solution with the sections was then heated to 80 °C for 90 min (PDW) or for 6 h (DW and DDW). After delignification, the sections were washed with deionized water until the pH value of the water reached 4.5 or higher. DDW sections were densified at 20 °C and 65 % RH between two metal sheets under a pressure of 20 MPa. For the microtensile tests, rectangular tensile specimens (length x width x thickness: 25 mm × 2 mm × ~0.04–0.1 mm) were cut from each section and preconditioned at room temperature (~22 °C) and a relative humidity similar to test conditions (70–80 % RH) for 30 to 60 min before testing.

At the μ-Spot beamline in BESSY II synchrotron radiation facilities, in-situ tensile tests were conducted and 32 measurements on specimens of Norway spruce (NW, PDW, DW and DDW) could be fully analysed

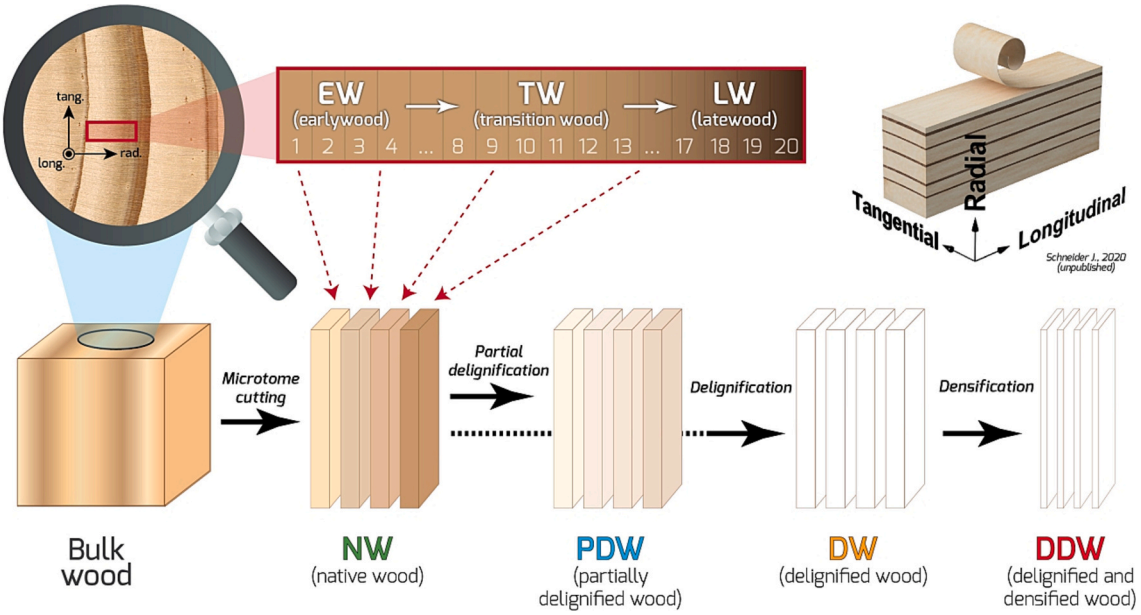

Fig. 1. Sample preparation from bulk wood to microtensile specimens.

(static tensile tests, 20 specimens; cycling loading tests, 12 specimens). The locations of specimens within the growth ring are compiled in Table 1.

2.2. Density measurements of samples

Densities were obtained from a segment directly next to the mechanically loaded sample on the same tangential cut. Dimensions were measured (thickness with a caliper (precision: 0.01 mm)) and the weighing of the sample was conducted with a precision scale (precision: 0.1 mg).

2.3. Moisture content measurements

Direct measurement of the moisture content of the tiny tested specimens was not possible with sufficiently high accuracy on site. Instead of this, we recorded temperature and relative humidity in the chamber of the microtensile testing machine and equilibrated the samples to these conditions. A temperature between 22 and 23 °C and a relative humidity between 70 and 80 % was recorded for all tested samples. Moisture content was measured on larger microtomed specimens collected from the same growth ring used for the mechanical tests. For each material (NW, PDW, DW, DDW), 5 to 6 specimens ranging from earlywood to latewood regions were conditioned in an environment close to the testing conditions. Constant climate (20 °C, 75 % relative humidity) was adjusted in a climate chamber and fully dried samples were obtained by drying in an oven at 103 °C. Finally, the masses of dry and moisturized specimens were used to calculate moisture contents, which are displayed in Fig. S2 in Supplementary material.

2.4. In-situ microtensile experiments combined with WAXD

In-situ microtensile tests combined with simultaneous WAXD measurements were carried out at the μ-Spot beamline (Paris et al., 2007) at the synchrotron radiation facilities BESSY II (Helmholtz Zentrum Berlin, Germany). A custom-built microtensile tester with simultaneous humidity control was mounted with the samples orientated perpendicular to the beam at a distance of 290 mm to the detector (schematic drawing, Fig. 2). Hereby, the X-rays passed through windows sealed with kapton foil. Specimens were loaded along their fiber direction at a constant test speed of 4 μm/s and forces were recorded with a 50 N load cell (Honeywell Sensotec). For cyclic testing, specimens were loaded until manually controlled force thresholds ranging from 1 to 27 N were reached. Increments between cycles were 0.5–3 N (data are shown in Supplementary material). The number of cycles until fracture ranged from 6 to 20 (9 in average) corresponding to test durations of 4 to 18 min while static tensile tests lasted typically 30 to 90 s.

Modulus of elasticity (MOE) and ultimate tensile strength (UTS) were calculated based on the cross sectional areas of the samples. The specific modulus of elasticity (sMOE) was determined by dividing the MOE by the respective sample density.

In order to measure deformation of crystalline cellulose upon microtensile loading, X-rays with a photon energy of 15 keV, corresponding to a wavelength of $\lambda = 0.8266$ Å, and a beam diameter of 100 μm were used. The WAXD signal was acquired using a Dectrix Eiger area detector (3108 × 3262 pixels, 75 μm pixel size) positioned at 290 mm distance from the sample. To minimize beam damage, specimens were scanned continuously along their width and length (mesh scan) and data were collected every ~3 s with 2 s of exposure to X-rays (more details in Supplementary material, Fig. S2).

2.5. Data processing

Two types of datasets were collected for each specimen: the microtensile dataset and the simultaneously obtained WAXD dataset. The microtensile dataset contains time [s], motor position [μm], force [N], temperature [°C] and relative humidity [% rh.] recorded at 5 Hz. The WAXD dataset consists of a collection of 2-D diffractograms in which each pixel is associated with an intensity value.

The collected WAXD diffractograms were processed with the analysis software DPDAK developed by DESY and the Max Planck Institute of Colloids and Interfaces (Benecke et al., 2014). For each diffractogram, air and background scattering (including scattering from the kapton foil) was removed by subtracting an "empty" diffractogram (image with kapton foil, but without sample). The diffractogram of aluminum oxide (Corundium) was used as calibration standard for determining beam center and sample-detector distance for calculating the scattering vector q as a function of the distance from the beam center in pixel. From the (004) Bragg reflections of the crystalline cellulose, intensity profiles as a function of q were extracted by azimuthal integration. A fit was applied to all curves using the Lorentz fit function included in DPDAK to determine q of the maximum intensity and the distance d of the corresponding lattice plane using Bragg's law. Fitted curves were then exported to MatLab, the shift of q was computed for each specimen and equivalent lattice strains of the crystalline cellulose were calculated according to the following equation.

$$\epsilon_{004} = \frac{d - d_0}{d_0} \qquad with\ d = \frac{n\lambda}{2sin\Theta} = \frac{n2\pi}{q}$$

with ϵ_{004} the lattice strain, d the current spacing of the crystal layers in the 004 direction, d_0 the initial spacing of the crystal layers in the 004 direction, λ the wavelength of the X-ray beam, Θ the scattering angle, q the scattering vector and n the diffraction order (here: 4).

The first evaluation of lattice strains showed fluctuations, which prevented us from accurately determining absolute lattice strain values for small deformation. These fluctuations are thought to be a consequence of the limited pixel resolution of the X-ray detector, possibly amplified by the beam relocation between every WAXD measurement on the sample. As an attempt to improve data readability, the resolution of data points in q-space was numerically increased ten-fold by applying spline interpolation (*interp1* function in MatLab®) to the q-intensity profiles.

To synchronize the microtensile test datasets and the WAXD measurements, the "first" (start of displacement) and "last" data point (fracture) of the tensile tests were determined numerically. The corresponding scan numbers of the collected diffractograms were manually documented during the experiment and data points within this range were further used for evaluation. The synchronization of the different data sampling rates (5 Hz for the microtensile tester and ~0.3 Hz for the

Table 1
Positions on the growth ring (GR) for tensile and cyclic specimens.

	GR position→	1	2	3	4	5	6	7	8	9	10	11	…	15	16	…	20
Static tensile tests (20 spec.)	NW			X		X		X		X		X	…			…	
	PDW	X	X		X		X		X		X		…			…	
	DW			X		X		X		X		X	…			…	
	DDW	X					X		X		X		…			…	
Cyclic tensile tests (12 spec.)	NW					X		X		X			…	X		…	
	PDW		X		X		X						…		X	…	
	DW			X		X		X					…		X	…	

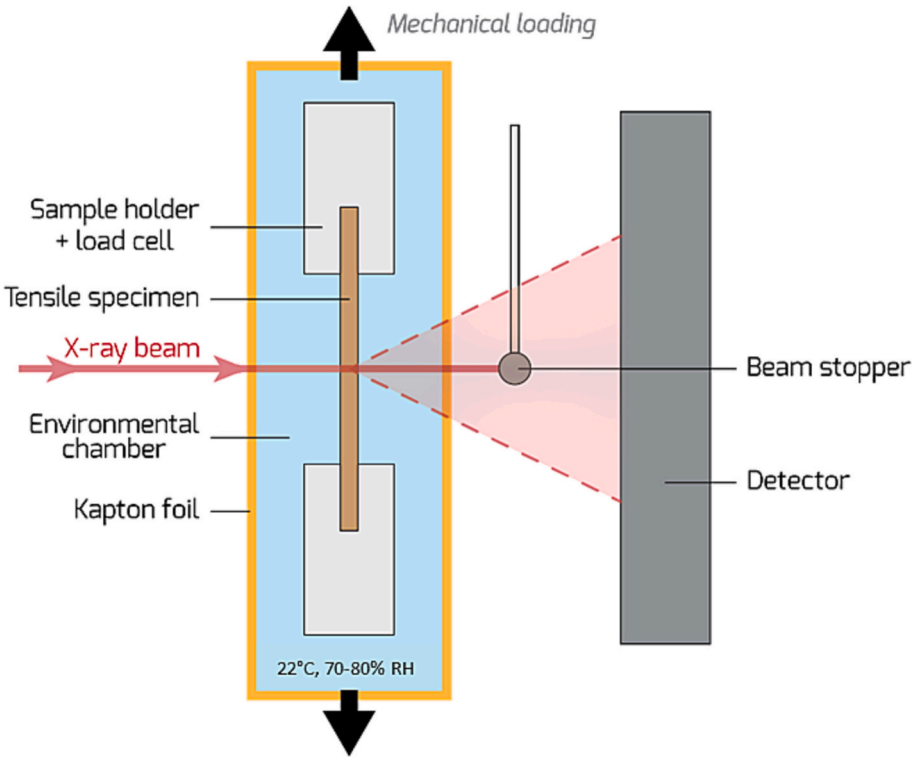

Fig. 2. In-situ microtensile setup combined with WAXD measurements.

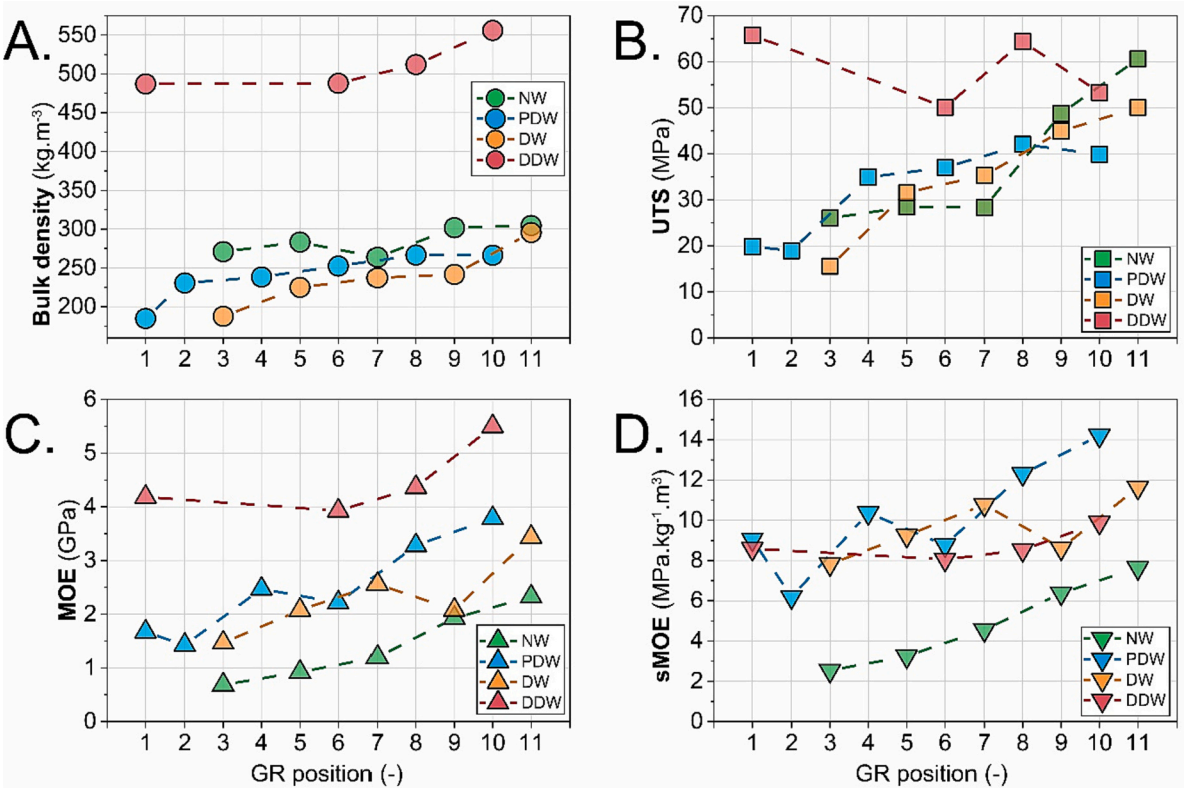

Fig. 3. Bulk density and mechanical properties of NW, PDW, DW and DDW tensile specimens collected from different positions of the same growth ring (GR). Dotted lines were added to guide the eye and highlight trends between specimens within the same material group.

diffractograms) was performed with MatLab®.

2.6. Statistical analysis

For all static tensile specimens, sMOE values and lattice strain slopes were checked for statistically significant differences ($p < 0.05$) by a one-factorial ANOVA test followed by a post-hoc test (Tukey test). These statistical tests were conducted on the following groups: *NW v PDW*, *NW v DW*, *NW v DDW*, *PDW v DW*, *PDW v DDW* and *DW v DDW*.

3. Results and discussion

3.1. Microtensile properties of native and treated samples

The thin native wood, (partly) delignified and densified specimens from different positions within the growth ring were loaded in static tensile tests in the test setup (Fig. 2). Bulk density, ultimate tensile strength (UTS), modulus of elasticity (MOE), and specific modulus of elasticity (sMOE) were determined (Fig. 3).

Fig. 3.A shows an increase in density with growth ring position from earlywood to transition wood for all four materials regardless of their treatments reflecting the gradual changes in cell size and cell wall thickness over the growth season. Earlywood cells formed at the beginning of the growth season (position 1 in Fig. 1) possess thin cell walls and large lumina for effective water transport in the living tree. Regions with thicker-walled cells and small lumina contribute more to the mechanical stability, apparent by higher MOE and UTS (Eder et al., 2008; Jyske et al., 2008). Although the growth ring positions range only from earlywood to the transition wood region, the increase of MOE and UTS in this direction is similar (except DDW, Fig. 3.B and C) to those observed in the literature for entire growth rings (Eder et al., 2008).

Compared to similar studies, MOE and UTS values (Fig. 3.B, C) are relatively low for Norway spruce (Frey et al., 2018; Jakob et al., 2020), which may be partly explained by the higher relative humidity in our testing environment (70–80 % RH). Additionally, a small size of a cellular sample is known to particularly affect the MOE, but also UTS (Andrews et al., 2001; Onck et al., 2001). Among non-densified specimens (i.e. NW, PDW, DW), lignin removal leads to a decrease in bulk density as well as an increase in MOE and sMOE, while leaving UTS almost unaffected. Additionally, a longer delignification time resulted in a stronger decrease in bulk density for DW compared to PDW. The decrease in bulk density without weakening of mechanical properties (or even increase for MOE) throughout delignification reflects the preservation of the structural integrity of the bulk material. Former studies using similar structure-retaining delignification strategies have also reported preservation or improvement of mechanical properties for chemically delignified wood (Frey, Schneider, et al., 2019; He et al., 2020; Yang et al., 2018).

Densified specimens (DDW) demonstrate significantly higher density, stiffness and tensile strength (for low growth ring positions only). Unlike non-densified specimens, UTS values for DDW specimens do not show a noticeable trend over the range of growth ring positions (Fig. 3.B). The behavior of DDW specimens is a direct consequence of the structural changes induced by densification treatment (Chen et al., 2020). Since the cell lumina collapse under transverse compressive loading, the density of the sample increases. The relative increase in density due to densification is more pronounced in earlywood regions due to the larger lumina compared to transition wood regions. Hence, the process of densification results in a homogenization of density and mechanical performance between different regions of the growth ring (Frey et al., 2018; Jakob et al., 2020).

The specific elastic modulus (sMOE) is commonly used in materials science and engineering to normalize MOE by density and compare the mechanical performance especially for lightweight materials (Ashby & Cebon, 2005). For wood as a porous material, the sMOE can give an indication of cell wall stiffness under the assumption of a rigid interface between fibers and pure loading in fiber direction. Fig. 3.D shows an increase of sMOE with growth ring position for all treatments, whereas the increase is most pronounced for NW and least for DDW. A higher sMOE with increasing growth ring position might be explained by a higher S2-layer proportion in thicker cell walls, since the S2 layer with a small microfibril angle is the main contributor to MOE and UTS (Reiterer et al., 1999). Furthermore, cell diameters get smaller across the growth ring, which may have resulted in a proportionally lower number of cut-open cells for the higher growth ring positions. The differences in sMOE between NW and delignified samples are possibly more related to the microstructure than to the nanostructure of the samples since cell wall MOEs of lignified and de-lignified single fibers were found to be similar (Eder et al., 2013).

The influence of the delignification treatment on mechanical properties also depends on the adjusted relative humidity, since hydrogen bonds connecting the cell wall polymers play a decisive role in the overall mechanical performance of wood (Alméras et al., 2017; Salmèn, 2009; Toba et al., 2013). Some studies suggest that the removal of the amorphous lignin-hemicelluloses matrix of the cell wall results in an increase of accessible OH groups on cellulose microfibrils. This could then lead to additional intermolecular hydrogen-bonds between microfibrils when pressed together (i.e. during densification) and, hence, improve wood mechanical performance (Song et al., 2018; Toba et al., 2013; Zhu et al., 2015). Therefore, the relative humidity of our testing environment (70–80 % RH) may impact stress-transfer at the cell wall level and between fibers by weakening interfacial hydrogen bonding. However, the average moisture contents measured afterwards on samples of the same growth ring, 9.2 % for NW, 9.4 % for PDW, 9.8 % for DW, 8.8 % for DDW (Fig. S2) are in the range of those at standard climate conditions, since a steeper rise in moisture content takes place beyond 80 % RH (Groenquist et al., 2019).

3.2. Multiscale analysis of deformation behavior

The lattice strain of crystalline cellulose was used to analyze the material response at the nanoscale, to gain a better understanding of the effects of delignification on stress-transfer mechanisms in wood. Tensile stress and lattice strain as functions of bulk strain are displayed in Fig. 4 for selected early- and transition wood specimens with different degrees of delignification and densification (all other data in Supplementary material).

The microtensile data of NW specimens (black curves in Fig. 4) indicate a complex mechanical behavior apparent by three distinct phases. The 1st phase demonstrates linear elastic behavior with a high slope followed by a 2nd phase, which is characterized by a decrease in slope. The 3rd phase starts with progressive stiffening towards a more linear behavior until fracture. Such a triphasic stress-strain behavior in tensile tests is known for wood specimens with a rather high microfibril angle in the S2 cell wall (Keckes et al., 2003; Köhler & Spatz, 2002). However, it might be also related to size effects, which have been observed in tensile test studies on thin wood samples and phloem fiber bundles with smaller microfibril angles in the cell walls (Baley, 2002; Navi et al., 1995; Placet, Cissé, & Boubakar, 2014; Placet, Trivaudey, et al., 2014). Indeed, the evaluation of the azimuthal profiles of the (200) Bragg peaks of the X-ray diffraction images revealed microfibril angles in the range of 5–10°. At the nanoscale (red scatter plots on Fig. 4 and Supplementary Fig. S3.1), the lattice- and bulk-strain plots for most of the NW samples also demonstrated three phases with a sequence of slopes similar to that of the macroscopic data. The 1st and 3rd phase are characterized by a high slope, which suggests efficient stress transfer to crystalline cellulose. During the 2nd phase, the slope is considerably lower, which highlights the reduction of stress-transfer to the crystalline regions of cellulose. At the wood tissue level, such behavior could be additionally attributed to shear slip occurring in the middle lamella.

In contrast to the mechanical behavior of the NW specimens, all (partly) delignified specimens showed more linear stress-strain curves as

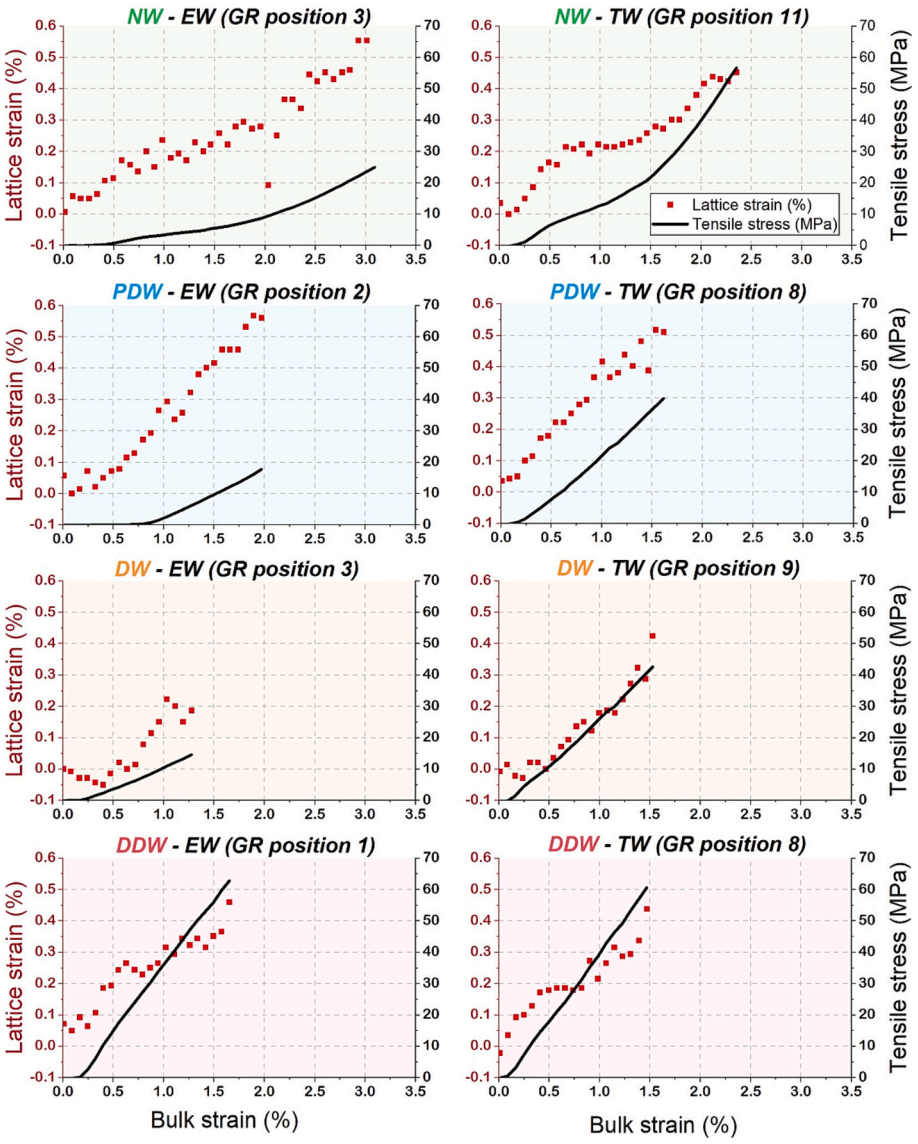

Fig. 4. Tensile stress - bulk strain curves (black solid lines) and lattice-strain – bulk strain scatter plots (red dots) for selected earlywood and transition wood samples (NW, PDW, DW and DDW). (For interpretation of the references to color in this figure legend, the reader is referred to the web version of this article.)

well as a reduced strain to failure. The average strain to failure and respective standard deviation for NW samples was 2.3 % (0.2 %), while it was 1.3 % (0.1 %) for PDW samples, 1.4 % (0.2 %) for DW samples, and 1.3 % (0.2 %) for DDW samples. The lower strain to failure of the delignified samples is in line with the lattice strain curves, which reach lower maximum lattice strain values compared to NW samples. This means that the fracture of delignified samples at lower strain levels impedes a further deformation of the crystalline regions of the cellulose fibrils. The lower strain to failure can be most probably explained by local defects as well as the reduction in density due to delignification leading to a removal of amorphous polymers, which are contributing to the stress transfer between cellulose fibrils.

The lattice strain curves of the delignified specimens are characterized by a single linear phase in most cases, but for a few specimens of PDW and DW and the majority of DDW samples these curves deviate from a linear slope. However, in contrast to NW, this does not seem to be directly coupled to global changes in stress-transfer mechanisms, but may indicate local differences due to inhomogeneous delignification treatment at the level of individual data acquisition spots. Generally, local effects may play a role, because the volume scanned by the X-ray beam during the in-situ tests is very small compared to that of the entire specimen and subsequent lattice strain values have been measured as a mesh scan of individual spots. Localized effects of the treatment will be further discussed when interpreting the correlation of sMOE and lattice strain curves and the behavior under cyclic loading.

Fig. 5 displays values of lattice strain slope (as a measure of the relationship between lattice strain and bulk strain and therefore reflecting stress transfer) and sMOE for all specimens tested in static in-situ tensile tests which allows for their direct comparison as a function of degree of delignification and densification and growth ring position.

The increasing sMOE with increasing growth ring position of NW specimens, which has already been discussed in the previous chapter, is positively correlated with lattice strain slope values (see LS slope/sMOE curve on NW sub-plot in Fig. 5). Since the elastic modulus of crystalline cellulose is much higher than that of the bulk wood or cell wall modulus, the lattice strain is a measure for the contribution of crystalline cellulose to the overall stiffness of bulk wood due to the stress transfer between cellulose fibrils and matrix components. Therefore, a higher sMOE should be in line with a higher lattice strain slope given that the cellulose-matrix interaction remains the same. Interestingly, this relationship is abolished by the delignification treatments. The statistical analysis revealed significantly higher sMOE for PDW and DW specimens

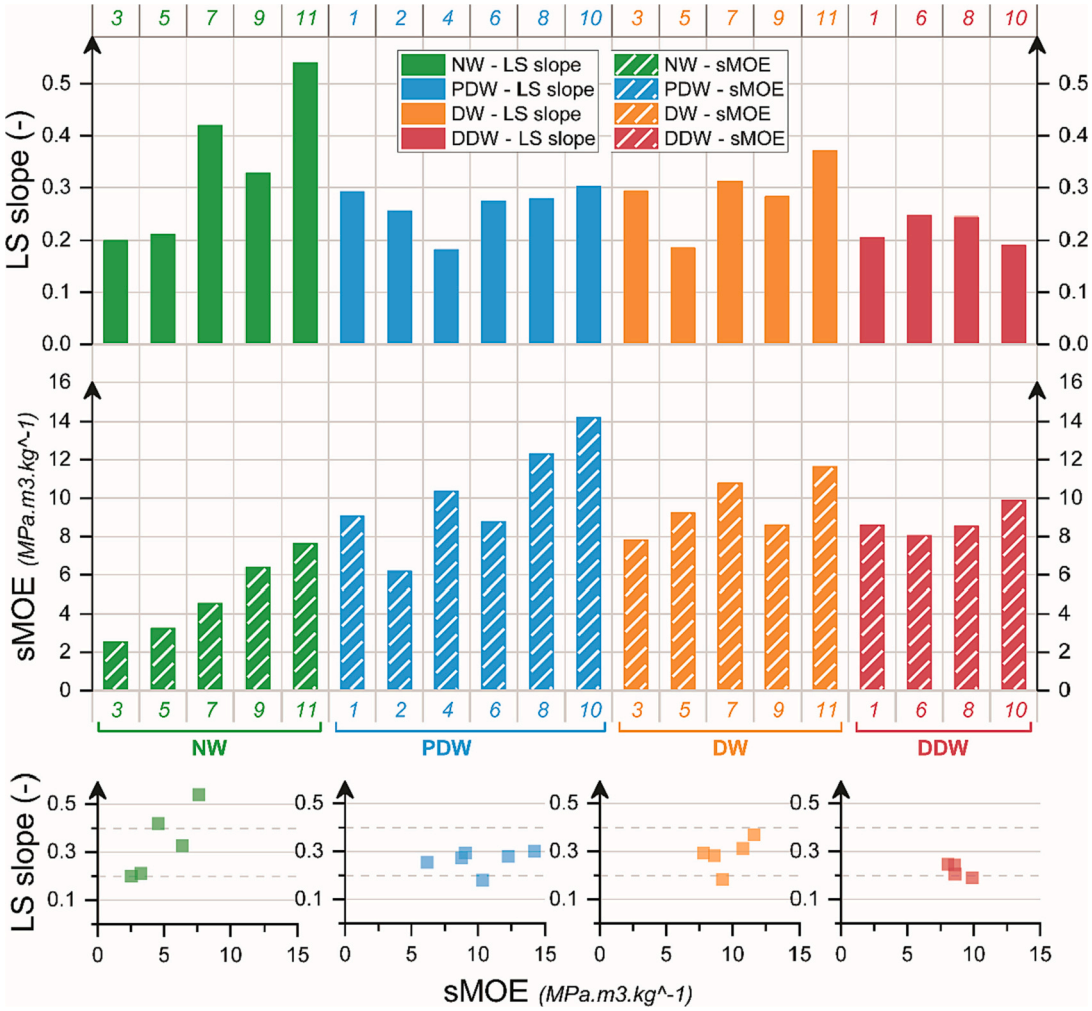

Fig. 5. Specific moduli of elasticity (sMOE) and LS slope values for all tensile specimens. Grouped by material, ordered by increasing growth ring position from left to right among the material group. For NW, the values displayed are the slopes of the 1st phase of the curves (i.e. before yield point).

in comparison to NW specimens (PDW: $p = 0.0065$; DW: $p = 0.0046$), yet no significant differences between DDW and NW specimens. Among all materials, statistical analysis revealed no significant differences for lattice strain slopes. Delignified samples stayed in the range of 0.2–0.3 with some variation for PDW and DW specimens. This indicates that delignification can significantly affect cell wall stiffness (represented by sMOE) while having no measurable influence on stress transfer to the crystalline cellulose (represented by LS slope). This could be explained by a superimposition of two compensatory effects caused by the delignification, namely the decomposition of the amorphous matrix, which should decrease the lattice strain ratio, and a geometrically tighter packing of cellulose fibrils, which would increase the stress transfer and, therefore, the lattice strain ratio. Focusing on the influence of growth ring position on the individual material, one can still observe an increasing trend of sMOE towards transition wood for PDW and possibly for DW, while the respective lattice strain slopes do not show any trend.

For DDW specimens, sMOE values are stable across growth ring positions, which confirms the homogenizing effect of densification on mechanical behavior. Lattice strain slopes of DDW specimens did not change compared to delignified specimens, indicating that additional densification does not lead to an improved stress-transfer to crystalline cellulose. Here, one needs to emphasize that only a rather mild densification was applied, resulting in a density in the range of 500 kg/m^3, which is only about half of density values obtained in other studies on delignified and densified wood (Frey et al., 2018). However, the unchanged lattice strain slopes indicate that the densification under the given treatment (mild densification) and testing conditions (70–80 % RH) only lead to a compaction at the cell level and did not affect the mechanical interaction of cellulose fibrils in the cell wall.

To gain further insight into the effect of the delignification on the multi-scale deformation behavior, we conducted additional cyclic tests. Stress-bulk strain curves, sMOE values and lattice strain slope values for NW, PDW and DW specimens with similar growth ring positions are presented in Fig. 6. Further cyclic stress-bulk strain curves as well as lattice strain – bulk strain curves can be found in Supplementary material. Tests until fracture comprised 6 to 20 cycles (9 in average), among which only the last 3 to 13 cycles (5 in average) showed a signal to noise ratio for the LS slope values high enough for further analysis.

Like already observed for the static in-situ tensile tests, the NW specimen showed a different stress-strain behavior during cyclic loading compared to the PDW and DW specimens. NW showed a pronounced change in slopes followed by a phase dominated by plastic deformation. Unloading and reloading resulted in a recurring almost linear phase with increasing slope in subsequent cycles. This behavior resembles wet compression wood tissue under cyclic loading, although the NW specimen in the present study showed less viscous contribution (Keckes et al., 2003). Contrary, PDW and DW possess almost no change in slope of the stress strain curve and the increase of stiffness from cycle to cycle is less pronounced.

When comparing the behavior in the last five cycles, NW specimens reveal sMOE values almost twice as high as those of the initial phase in

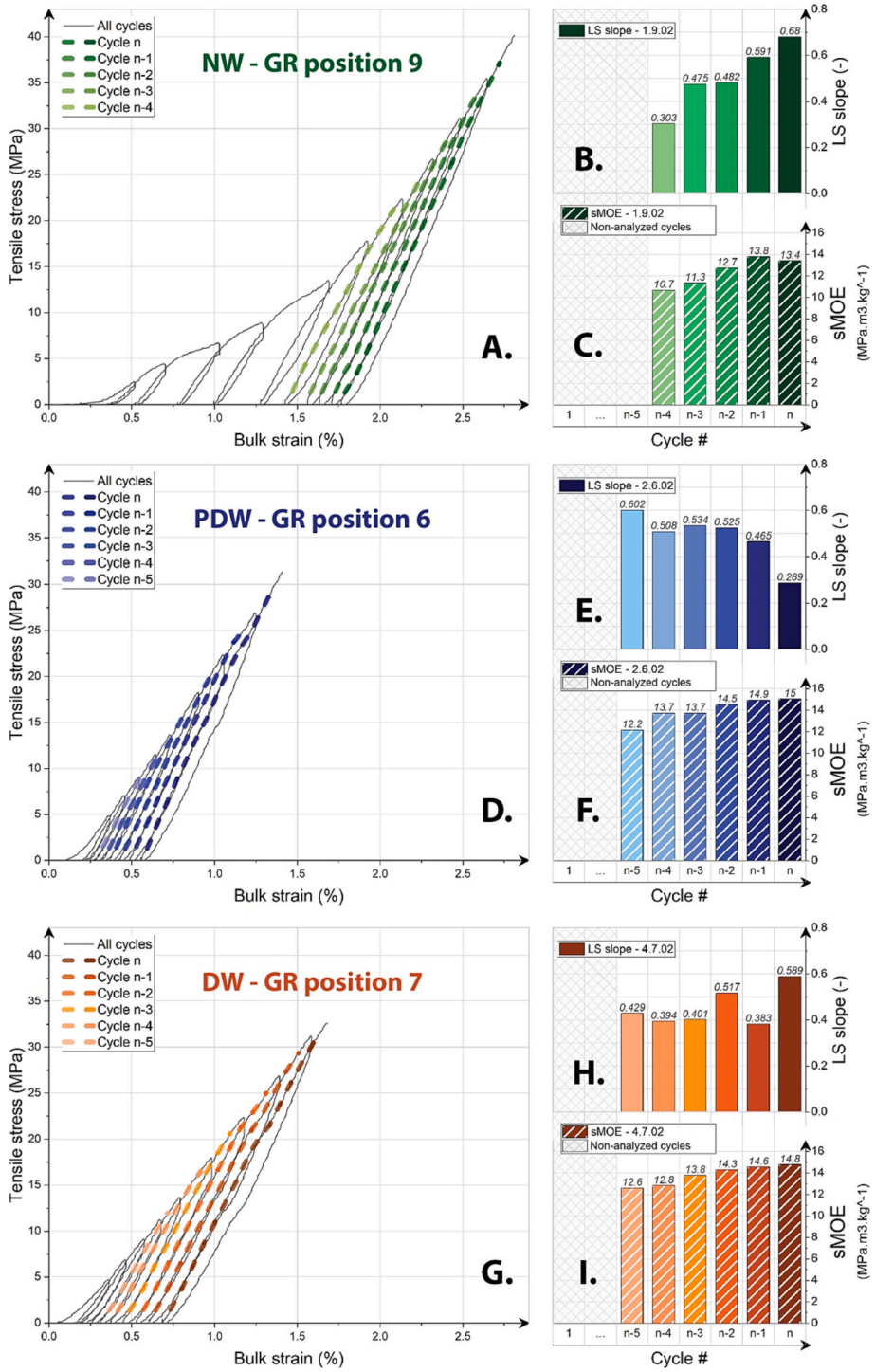

Fig. 6. Cyclic study: Evolution of the specific modulus of elasticity (sMOE) and of the slope of the lattice strain (LS) as a function of bulk strain (BS) during cyclic microtensile tests.

the static tests (Fig. 3. similar growth ring position). Accordingly, the lattice strain slopes are substantially higher than those of the static tests. The analysis of the last cycles of PDW and DW specimens revealed in turn higher values of sMOE compared to those of NW at least in some cases (not visible in Fig. 6, but in Supplementary material) as it has already been observed for the static tests (Fig. 5). Yet, the lattice strain slope values are comparable to those of NW specimens confirming the rather limited importance of the cell wall matrix for this specific test configuration (small microfibril angle, 70–80 % RH).

Following a more detailed analysis of the last cycles, lattice strain slopes and sMOE show a consistent trend to higher values with increasing cycle number for NW (Fig. 6.A and B). The stiffening effect of the cyclic loading may be explained by a progressive alignment of cellulose fibrils and a reduction of the viscous component of deformation, which is also reflected by the increased lattice strain slope values. PDW and DW specimens also show an increase in sMOE for subsequent loading cycles. In contrast to NW specimens, no consistent trend of lattice strain slope values is visible for subsequent loading cycles in PDW and DW samples (Fig. 6 and Supplementary material). For PDW, the data analysis shown in Fig. 6 displays a decrease of lattice strain slopes, but

this is not representative for this parameter, since other specimens with the same treatment showed a different lattice strain slope pattern without any trend in the last cycles (see Supplementary material). Likewise, the lattice strain slope values of DW do not show a specific trend across the last cycles.

These findings are in accordance with the interpretation of the static in-situ test data suggesting a decoupling of trends in sMOE and cellulose crystal deformation due to the delignification treatments. Since lignin is removed from the cell wall and from the middle lamella, which is gluing the fibers together, structural and chemical changes between fibers and/or at the cell wall level could affect sMOE and lattice strain slope. This cannot be distinguished with the chosen in-situ testing protocol, as it would require additional tests on individual fibers (Keckes et al., 2003). However, the stress-strain curves of PDW and DW do not indicate a gliding between fibers as this would lead to pronounced plastic deformation. At the cell wall level it seems reasonable to assume that delignification treatments increase the freedom of spatial reorientation of cellulose fibrils. This should facilitate axial alignment of fibrils already in the initial load cycles and may explain the comparably high sMOEs values in the last six cycles with only rather little further increase during these cycles. Particularly PDW samples showed no specific trend of lattice strain slopes, but a considerable scatter of the values in the individual cycles, which could be explained by an inhomogeneous delignification in PDW samples with some locations retained more or less degraded lignin components with a local impact on the stress transfer to the cellulose fibrils eventually obscuring a global trend. In terms of fully delignified specimens (DW) the observed scatter of values in lattice strain slopes cannot originate from remaining lignin moieties, but may stem from different degrees of degradation or alteration of hemicelluloses and cellulose fibril surfaces.

4. Conclusion

We gained insights into stress transfer mechanisms of wood cell walls by mechanically loading small specimens of untreated (NW), partly delignified (PDW), delignified (DW) and delignified and densified (DDW) wood with simultaneous synchrotron X-ray diffraction analysis at 70–80 % relative humidity. Cell wall stiffness in terms of specific modulus of elasticity (sMOE) was compared with the ratio of lattice strain of the crystalline cellulose to bulk strain of the specimen, which we termed lattice strain slope. A consistent trend of sMOE and lattice strain slope was found for NW. In contrast, higher values of sMOE of PDW and DW specimens compared to NW did not result in higher values of lattice strain slope of these treated samples. This may be explained by an inhomogeneous spatial delignification or indicate that, at the adjusted relative humidity, a closer arrangement of cellulose fibrils due to lignin (and hemicelluloses) removal does not result in a more efficient stress transfer in the cell wall. Therefore, our hypothesis that the stress transfer would be significantly changed by delignification cannot be confirmed. This may be explained by a compensatory effect counterbalancing the decomposition of the amorphous matrix by delignification (that should decrease the strain ratio) and a geometrically tighter packing of cellulose crystals that would increase the stress transfer and, therefore, the strain ratio. Moreover, the delignified specimens reach lower maximum lattice strain values compared to normal wood, because of a fracture at lower bulk strain levels. This is most probably caused by structural defects and/or the removal of the amorphous polymers. In future studies, it would be well worth investigating the behavior of untreated and delignified wood also in dry conditions and after stronger densification, since both should result in a tighter cellulose packing.

CRediT authorship contribution statement

Paul-Antoine Spies: Methodology, Validation, Formal analysis, Investigation, Writing – original draft, Visualization. **Tobias Keplinger:** Conceptualization, Formal analysis, Investigation. **Nils Horbelt:** Formal analysis, Investigation, Writing – review & editing. **Friedrich Reppe:** Formal analysis, Investigation. **Ernesto Scoppola:** Formal analysis, Investigation. **Michaela Eder:** Conceptualization, Investigation, Formal analysis, Methodology, Writing – review & editing. **Peter Fratzl:** Conceptualization, Formal analysis, Methodology, Resources, Writing – review & editing, Project administration. **Ingo Burgert:** Conceptualization, Methodology, Formal analysis, Resources, Writing – review & editing, Supervision, Project administration. **Markus Rüggeberg:** Conceptualization, Methodology, Investigation, Formal analysis, Writing – review & editing.

Declaration of competing interest

The authors declare that they have no known competing financial interests or personal relationships that could have appeared to influence the work reported in this paper.

Data availability

Data will be made available on request.

Acknowledgments

We thank Marion Frey for sample preparation.

Funding

The project was conducted in the framework of the SNF project “Hierarchical cellulose scaffolds for structural and functional gradient materials” (200021_184821/1). ME and PF acknowledge the support of the Cluster of Excellence “Matters of Activity. Image Space Material” funded by the Deutsch Forschungsgemeinschaft (DFG, German Research Foundation) under Germany's Excellence Strategy – EXC 2025-390648296. ES, FR, ME, NH and PF are grateful for the support of the Max Planck Society.

Appendix A. Supplementary data

Supplementary data to this article can be found online at https://doi.org/10.1016/j.carbpol.2022.119922.

References

Alméras, T., Gronvold, A., van der Lee, A., Clair, B., & Montero, C. (2017). Contribution of cellulose to the moisture-dependent elastic behaviour of wood. *Composites Science and Technology, 138*, 151–160. https://doi.org/10.1016/j.compscitech.2016.11.025

Andrews, E. W., Gioux, G., Onck, P., & Gibson, L. J. (2001). Size effects in ductile cellular solids. Part II: Experimental results. *International Journal of Mechanical Sciences, 43*(3), 701–713. https://doi.org/10.1016/S0020-7403(00)00043-6

Ashby, M. F., & Cebon, D. (2005). Materials selection in mechanical design. *MRS Bulletin, 30*(12), 995.

Baley, C. (2002). Analysis of the flax fibres tensile behaviour and analysis of the tensile stiffness increase. *Composites Part A Applied Science and Manufacturing*. https://doi.org/10.1016/S1359-835X(02)00040-4

Benecke, G., Wagermaier, W., Li, C., Schwartzkopf, M., Flucke, G., Hoerth, R., … Fratzl, P. (2014). A customizable software for fast reduction and analysis of large X-ray scattering data sets: Applications of the new DPDAK package to small-angle X-ray scattering and grazing-incidence small-angle X-ray scattering. *Journal of Applied Crystallography, 47*(5), 1797–1803. https://doi.org/10.1107/S1600576714019773

Chen, C., Kuang, Y., Zhu, S., Burgert, I., Keplinger, T., Gong, A., … Hu, L. (2020). Structure–property–function relationships of natural and engineered wood. *Nature Reviews Materials, 5*(9), 642–666. https://doi.org/10.1038/s41578-020-0195-z

Conrad, M. P. C., Smith, G. D., & Fernlund, G. (2003). Fracture of solid wood: A review of structure and properties at different length scales. *Wood and Fiber Science, 35*(4), 570–584.

Diddens, I., Murphy, B., Krisch, M., & Müller, M. (2008). Anisotropic elastic properties of cellulose measured using inelastic X-ray scattering. *Macromolecules, 41*(24), 9755–9759. https://doi.org/10.1021/ma801796u

Eder, M., Arnould, O., William, J., Dunlop, C., Hornatowska, J., & Salmen, L. (2013). Experimental micromechanical characterisation of wood cell walls. *Wood Science and Technology, 47*(1), 163–182. https://doi.org/10.1007/s00226-012-0515-6

Eder, M., Terziev, N., Daniel, G., & Burgert, I. (2008). The effect of (induced) dislocations on the tensile properties of individual Norway spruce fibres. *Holzforschung, 62*(1), 77–81. https://doi.org/10.1515/HF.2008.011

Engelund, E. T., Thygesen, L. G., Svensson, S., & Hill, C. A. S. (2013). A critical discussion of the physics of wood-water interactions. *Wood Science and Technology, 47*(1), 141–161. https://doi.org/10.1007/s00226-012-0514-7

Felhofer, M., Bock, P., Singh, A., Prats-Mateu, B., Zirbs, R., & Gierlinger, N. (2020). Wood deformation leads to rearrangement of molecules at the nanoscale. *Nano Letters, 20*(4), 2647–2653. https://doi.org/10.1021/acs.nanolett.0c00205

Frey, M., Biffi, G., Adobes-Vidal, M., Zirkelbach, M., Wang, Y., Tu, K., … Keplinger, T. (2019). Tunable wood by reversible interlocking and bioinspired mechanical gradients. *Advanced Science, 6*(10). https://doi.org/10.1002/advs.201802190

Frey, M., Schneider, L., Masania, K., Keplinger, T., & Burgert, I. (2019). Delignified wood-polymer interpenetrating composites exceeding the rule of mixtures. *ACS Applied Materials and Interfaces, 11*(38), 35305–35311. https://doi.org/10.1021/acsami.9b11105

Frey, M., Widner, D., Segmehl, J. S., Casdorff, K., Keplinger, T., & Burgert, I. (2018). Delignified and densified cellulose bulk materials with excellent tensile properties for sustainable engineering. *ACS Applied Materials and Interfaces, 10*(5), 5030–5037. https://doi.org/10.1021/acsami.7b18646

Gibson, L. J. (2012). The hierarchical structure and mechanics of plant materials. *Journal of the Royal Society Interface, 9*(76), 2749–2766. https://doi.org/10.1098/rsif.2012.0341

Gierlinger, N., Schwanninger, M., Reinecke, A., & Burgert, I. (2006). Molecular changes during tensile deformation of single wood fibers followed by Raman microscopy. *Biomacromolecules, 7*(7), 2077–2081. https://doi.org/10.1021/bm060236g

Groenquist, P., Frey, M., Keplinger, T., & Burgert, I. (2019). Mesoporosity of delignified wood investigated by water vapor sorption. *ACS Omega, 4*, 12425–12431.

Han, X., Ye, Y., Lam, F., Pu, J., & Jiang, F. (2019). Hydrogen-bonding-induced assembly of aligned cellulose nanofibers into ultrastrong and tough bulk materials. *Journal of Materials Chemistry A, 7*(47), 27023–27031. https://doi.org/10.1039/c9ta11118b

He, S., Chen, C., Li, T., Song, J., Zhao, X., Kuang, Y., … Hu, L. (2020). An energy-efficient, wood-derived structural material enabled by pore structure engineering towards building efficiency. *Small Methods, 4*(1), 1–8. https://doi.org/10.1002/smtd.201900747

Jakob, M., Stemmer, G., Czabany, I., Müller, U., & Gindl-Altmutter, W. (2020). Preparation of high strength plywood from partially delignified densified wood. *Polymers, 12*(8). https://doi.org/10.3390/polym12081796

Jungnikl, K., Paris, O., Fratzl, P., & Burgert, I. (2008). The implication of chemical extraction treatments on the cell wall nanostructure of softwood. *Cellulose, 15*(3), 407–418. https://doi.org/10.1007/s10570-007-9181-5

Jyske, T., Mäkinen, H., & Saranpää, P. (2008). Wood density within Norway spruce stems. *Silva Fennica, 42*(3), 439–455. https://doi.org/10.14214/sf.248

Kamiyama, T., Suzuki, H., & Sugiyama, J. (2005). Studies of the structural change during deformation in Cryptomeria japonica by time-resolved synchrotron small-angle X-ray scattering. *Journal of Structural Biology, 151*(1), 1–11. https://doi.org/10.1016/j.jsb.2005.04.007

Keckes, J., Burgert, I., Frühmann, K., Müller, M., Kölln, K., Hamilton, M., … Fratzl, P. (2003). Cell-wall recovery after irreversible deformation of wood. *Nature Materials, 2*(12), 810–814. https://doi.org/10.1038/nmat1019

Keplinger, T., Wittel, F. K., Rüggeberg, M., & Burgert, I. (2020). Wood derived cellulose scaffolds—Processing and mechanics. *Advanced Materials, 2001375*, 1–19. https://doi.org/10.1002/adma.202001375

Klauditz, W. (1952). Zur biologisch-mechanischen Wirkung des Lignins im Stammholz der Nadel- und Laubhölzer. *Holzforschung, 6*(3), 70–82. https://doi.org/10.1515/hfsg.1952.6.3.70

Köhler, L., & Spatz, H. C. (2002). Micromechanics of plant tissues beyond the linear-elastic range. *Planta, 215*(1), 33–40. https://doi.org/10.1007/s00425-001-0718-9

Kölln, K., Grotkopp, I., Burghammer, M., Roth, S. V., Funari, S. S., Dommach, M., & Müller, M. (2005). Mechanical properties of cellulose fibres and wood. Orientational aspects in situ investigated with synchrotron radiation. *Journal of Synchrotron Radiation, 12*(6), 739–744. https://doi.org/10.1107/S0909049505011714

Müller, M., Krasnov, I., Ogurreck, M., Blankenburg, M., Pazera, T., & Seydel, T. (2011). Wood and silk: Hierarchically structured biomaterials investigated in situ with X-ray and neutron scattering. *Advanced Engineering Materials, 13*(8), 767–772. https://doi.org/10.1002/adem.201000347

Nakai, T., Yamamoto, H., & Nakao, T. (2005). The relationship between macroscopic strain and crystal lattice strain in wood under uniaxial stress in the fiber direction. *Journal of Wood Science, 51*(2), 193–194. https://doi.org/10.1007/s10086-005-0697-8

Nakai, T., Yamamoto, H., Nakao, T., & Hamatake, M. (2006). Mechanical behavior of the crystal lattice of natural cellulose in wood under repeated uniaxial tension stress in the fiber direction. *Wood Science and Technology, 40*(8), 683–695. https://doi.org/10.1007/s00226-006-0095-4

Navi, P., Rastogi, P. K., Gresse, V., & Tolou, A. (1995). Micromechanics of wood subjected to axial tension. *Wood Science and Technology, 29*(6), 411–429. https://doi.org/10.1007/BF00194199

Onck, P. R., Andrews, E. W., & Gibson, L. J. (2001). Size effects in ductile cellular solids. Part I: Modeling. *International Journal of Mechanical Sciences, 43*(3), 681–699. https://doi.org/10.1016/S0020-7403(00)00042-4

Özparpucu, M., Gierlinger, N., Cesarino, I., Burgert, I., Boerjan, W., & Rüggeberg, M. (2019). Significant influence of lignin on axial elastic modulus of poplar wood at low microfibril angles under wet conditions. *Journal of Experimental Botany, 70*(15), 4039–4047. https://doi.org/10.1093/jxb/erz180

Paris, O., Li, C., Siegel, S., Weseloh, G., Emmerling, F., Riesemeier, H., Erko, A., & Fratzl, P. (2007). A new experimental station for simultaneous X-ray microbeam scanning for small- and wide-angle scattering and fluorescence at BESSY II. *Journal of Applied Crystallography, 40*, 466–470. https://doi.org/10.1107/S0021889806045444

Peura, M., Kölln, K., Grotkopp, I., Saranpää, P., Müller, M., & Serimaa, R. (2007). The effect of axial strain on crystalline cellulose in Norway spruce. *Wood Science and Technology, 41*(7), 565–583. https://doi.org/10.1007/s00226-007-0141-x

Placet, V., Cissé, O., & Boubakar, L. (2014). Nonlinear tensile behaviour of elementary hemp fibres. Part I: Investigation of the possible origins using repeated progressive loading with in situ microscopic observations. *Composites Part A: Applied Science and Manufacturing, 56*, 319–327. https://doi.org/10.1016/j.compositesa.2012.11.019

Placet, V., Trivaudey, F., Cissé, O., & Boubakar, L. (2014). *What are the possible origins of the nonlinear tensile behaviour of hemp fibres? The 19th International Conference on Composite Materials (ICCM), Jan 2013, France* (pp. 1–8) (ffhal-01002412f).

Reiterer, A., Lichtenegger, H., Tschegg, S., & Fratzl, P. (1999). Experimental evidence for a mechanical function of the cellulose microfibril angle in wood cell walls. *Philosophical Magazine A: Physics of Condensed Matter, Structure, Defects and Mechanical Properties, 79*(9), 2173–2184. https://doi.org/10.1080/01418619908210415

Rowell, R. M. (2005). *Handbook of wood chemistry and wood composites*.

Salmén, L. (2004). Micromechanical understanding of the cell-wall structure. *Comptes Rendus Biologies, 327*(9–10), 873–880. https://doi.org/10.1016/j.crvi.2004.03.010

Salmèn, L. (2009). Cell wall features with regard to mechanical performance. A review. COST Action E35 2004–2008: Wood machining – micromechanics and fracture. *63*, 121–129. https://doi.org/10.1515/HF.2009.011

Salmén, L. (2018). Wood cell wall structure and organisation in relation to mechanics. *Plant Biomechanics: From Structure to Function at Multiple Scales, 3–19*. https://doi.org/10.1007/978-3-319-79099-2_1

Salmèn, L., & Bergström, E. (2009). Cellulose structural arrangement in relation to spectral changes in tensile loading FTIR. *Cellulose, 16*, 975–982. https://doi.org/10.1007/s10570-009-9331-z

Segmehl, J. S., Studer, V., Keplinger, T., & Burgert, I. (2018). Characterization of wood derived hierarchical cellulose scaffolds for multifunctional applications. *Materials, 11*(4), 1–11. https://doi.org/10.3390/ma11040517

Shams, M. I., Yano, H., & Endou, K. (2004). Compressive deformation of wood impregnated with low molecular weight phenol formaldehyde (PF) resin I: Effects of pressing pressure and pressure holding. *Journal of Wood Science, 50*(4), 337–342. https://doi.org/10.1007/s10086-003-0570-6

Song, J., Chen, C., Zhu, S., Zhu, M., Dai, J., Ray, U., … Hu, L. (2018). Processing bulk natural wood into a high-performance structural material. *Nature, 554*(7691), 224–228. https://doi.org/10.1038/nature25476

Stanzl-Tschegg, S. E. (2011). Wood as a bioinspiring material. *Materials Science and Engineering C, 31*(6), 1174–1183. https://doi.org/10.1016/j.msec.2010.12.001

Thygesen, L. G., Tang Engelund, E., & Hoffmeyer, P. (2010). Water sorption in wood and modified wood at high values of relative humidity. Part I: Results for untreated, acetylated, and furfurylated Norway spruce. *Holzforschung, 64*(3), 315–323. https://doi.org/10.1515/HF.2010.044

Toba, K., Yamamoto, H., & Yoshida, M. (2013). On the mechanical interaction between cellulose microfibrils and matrix substances in wood cell walls: Effects of chemical pretreatment and subsequent repeated dry-and-wet treatment. *Journal of Wood Science, 59*(5), 359–366. https://doi.org/10.1007/s10086-013-1347-1

Yang, X., Berthold, F., & Berglund, L. A. (2018). Preserving cellulose structure: Delignified wood fibers for paper structures of high strength and transparency. *Biomacromolecules, 19*(7), 3020–3029. https://doi.org/10.1021/acs.biomac.8b00585

Zabler, S., Paris, O., Burgert, I., & Fratzl, P. (2010). Moisture changes in the plant cell wall force cellulose crystallites to deform. *Journal of Structural Biology, 171*(2), 133–141. https://doi.org/10.1016/j.jsb.2010.04.013

Zhang, C., Chen, M., Keten, S., Coasne, B., Derome, D., & Carmeliet, J. (2021). Hygromechanical mechanisms of wood cell wall revealed by molecular modeling and mixture rule analysis. *Science Advances, 7*(37), 1–18. https://doi.org/10.1126/sciadv.abi8919

Zhu, H., Zhu, S., Jia, Z., Parvinian, S., Li, Y., Vaaland, O., Hu, L., & Li, T. (2015). Anomalous scaling law of strength and toughness of cellulose nanopaper. *Proceedings of the National Academy of Sciences of the United States of America, 112*(29), 8971–8976. https://doi.org/10.1073/pnas.1502870112